Nanometer Stepping Drives of Surface Acoustic Wave Motor

Takashi Shigematsu, *Student Member, IEEE*, Minoru Kuribayashi Kurosawa, *Member, IEEE*, and Katsuhiko Asai

***Abstract*—High resolution (from nanometer to subnanometer) stepping drives of a surface acoustic wave motor are presented. It was shown that step displacement was easily controlled by adjusting a number of driving waves, using a steel ball slider equipped with permanent magnet for preload. By means of this open loop control, the step displacement was controlled from centimeter-order to submicrometer-order. In this paper, using a silicon slider equipped with a ball bearing linear guide, the stepping motions of a surface acoustic wave motor were investigated. A laser interferometer equipped with a 2-picometer resolution displacement demodulator was introduced. Motions of the slider ranging from several hundreds of nanometers to several nanometers in each step displacement were observed.**

Reduction of the driving waves down to 25 cycles, under a 100 V_{peak} driving voltage and a 30 N preload condition, generated about 2 nm stepping motion using our experimental setup under an open loop condition. We also demonstrated subnanometer step movements. These experimental results indicated that the surface acoustic wave motor has an ability of subnanometer positioning with a centimeter-level stroke.

I. Introduction

Ultrasonic motors use mechanical vibration and frictional force between solid materials. The mechanical vibration is excited by piezoelectric material in a transducer. Owing to the large output forces of piezoelectric transducers, the thrusts or torques of ultrasonic motors are relatively large. The high output force and the low compliance structure due to the friction drive make ultrasonic motors suitable for high-speed and high-resolution positioning systems.

Usually, ultrasonic motors are operated at a resonance frequency of several tens of kilohertz. Independent to the driving frequency, vibration velocities ranging from several millimeters per second to several meters per second were used. The vibration amplitudes, therefore, range from several tens of nanometers to several micrometers. The limit of motion resolution seems to be dependent on the vibration amplitude of an ultrasonic transducer. Hence, the stepping motion resolution of an ultrasonic motor is limited to a submicrometer or a tenth of this, with the resolution of a common ultrasonic motor having been reported down to several tens of nanometers [1]. To obtain much higher resolution, direct current (DC) operation of the piezo actuators has been applied to a rotation motor [2] and to a linear motor [3]. For this driving method, however, two kinds of electrical sources are required and wasteful switching time is needed for an actual control system.

In order to maintain precision of positioning, a stator of an ultrasonic motor must be rigidly held. The stator vibrates itself; however, the holding mechanism of the stator is frequently a problem [4]. For the rigid retention of the stator, the stator should possess a nonvibrating part in its vibrating body to allow it to be held, under resonant conditions. However, this nonvibrating part has not been designed, except for a few examples [5].

The surface acoustic wave motor provides solutions to these problems. A surface acoustic wave device, in which the surface acoustic wave motor is used as the stator, is operated at approximately 10 MHz. The driving frequency is more than 100 times higher than that of the transducers used in the common ultrasonic motors. Therefore, the vibration amplitude of the surface acoustic wave device is more than 100 times smaller under the same vibration velocity conditions. The vibration amplitude ranges from subnanometer to a few tens of nanometers, if the vibration velocity ranges from several millimeters per second to several meters per second. Hence, the expected motion resolution is on the subnanometer scale [6], [7].

The nonvibrating parts of a surface acoustic wave device are also advantageous for precise positioning. The device generates the surface acoustic wave only on one plane, and it shows almost no vibrations at the bottom and side walls of the device. These nonvibrating parts are rigidly held to prevent the fluctuation of the entire motor. In other words, the surface acoustic wave motor is of very low compliance. This low compliance structure will be able to realize precise and accurate positioning.

Basic characteristics such as the speed and output force of the same type of transducer have been reported in other papers [8], [9]. As well, the high-resolution stepping drive motions of the motor also have been reported. But due to the technical limitations of measurement equipment, we have reported only 40 nm [10] and 25 nm [11] stepping drive motions. The present paper describes the stepping drives of a surface acoustic wave motor, down to a subnanometer-order, measured using a laser Doppler in-

Manuscript received June 5, 2002; accepted October 31, 2002. This work was supported by a Grant-in-Aid for the Development of Innovative Technology of the Ministry of Education, Culture, Sports, Science and Technology of Japan.

T. Shigematsu and M. K. Kurosawa are affiliated with the Interdisciplinary Graduate School of Engineering, Tokyo Institute of Technology, Yokohama, Japan (e-mail: tucker@ae.titech.ac.jp).

K. Asai is affiliated with Advanced Technology Research Laboratories, Matsushita Electric Industrial Co., Ltd., Kyoto, Japan.

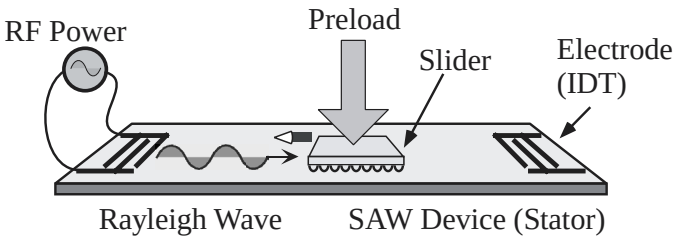

Fig. 1. Schematic view of a surface acoustic wave motor.

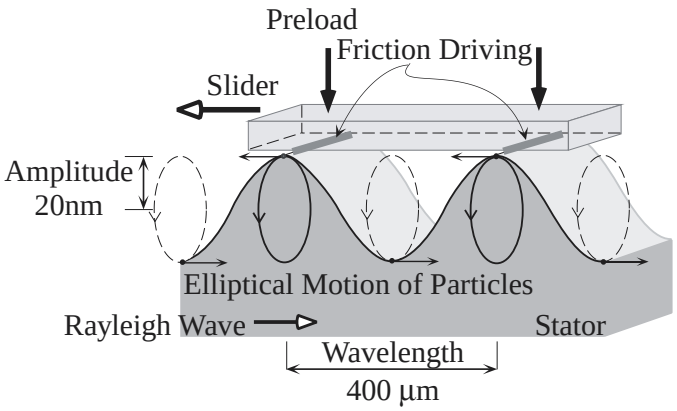

Fig. 2. Friction drive mechanism of a surface acoustic wave motor.

terferometer equipped with a 2-picometer resolution displacement demodulator.

II. Principle

A surface acoustic wave motor is a traveling wave-type ultrasonic motor using a Rayleigh wave. A stator made of a piezoelectric material has two interdigital transducers (IDTs) at both end ports of a substrate as shown in Fig. 1. From one IDT, a Rayleigh wave is generated by means of the piezoelectric effect using a radio frequency (RF) electrical power source. The progressive Rayleigh wave is converted to unidirectional slider motion through frictional force. A preload is applied to the slider in order to increase the motor's output force. By using the opposite side IDT, the slider motion is reversed.

The details of the friction drive mechanism are illustrated in Fig. 2. Surface particles of the stator move elliptically. Contacts of the stator with the slider then are made around wave crests. At the wave crests, the particles have a maximum horizontal velocity component. This particle motion is transmitted to the slider through frictional force.

For example, as shown in Fig. 2, the amplitude of a Rayleigh wave is 20 nm at most, and its wavelength is 400 μm. That is, the stator surface is almost flat. This small fluctuation acts as both an aid and a hindrance in a surface acoustic wave motor. One hindrance is difficulty of the contact between a stator and a slider [7]. However, the nanometer amplitude will bring a distinctive advantage

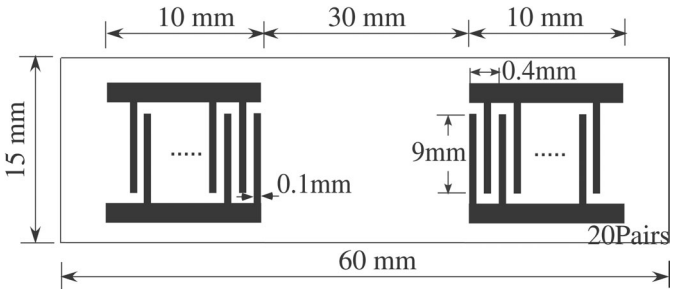

Fig. 3. Geometry of the stator and IDTs.

for nanometer stepping drives of a surface acoustic wave motor.

To enlarge the frictional force between the slider and the particles' Rayleigh wave motion, a preload is applied to the slider. The frictional force increases with the preload. As a result, the output force of the motor increases with the preload to a certain point [12].

III. Experimental Setup

A stator was a rectangular plate of 128 degrees y-rotated x-propagation $LiNbO_3$ substrate. The dimensions of the stator were $60 \times 15 \times 1$ mm^3. At each end of the stator, IDTs were fabricated by means of the deposition as shown in Fig. 3. The electrode materials were chromium and aluminum. The dimensions of the IDTs were 400 μm in pitch, 100 μm in electrode strip width, and 9 mm in aperture. Each IDT was composed of 20 strip electrode pairs, and the resonance frequency for Rayleigh wave propagation was 9.6 MHz.

The contact condition between a stator and a slider is crucial in a surface acoustic wave motor [13], because the squeezed air film disturbs the friction drive [14]. Hence, a silicon slider fabricated with projections on its contact surface has been used to eliminate the squeezed air film effect [15]. An experimental silicon slider was a square plate of silicon substrate. The dimensions of the silicon slider were $5 \times 5 \times 0.6$ mm^3. Numbers of 10,000 cylindrical projections were fabricated in a 4×4 mm^2 central square region of the surface by means of the dry-etching process. The cylindrical projections were 20 μm in diameter, 2 μm in height, and arranged at a 40 μm pitch. A scanning electron micrograph (SEM) photograph of the contact surface of the silicon slider is shown in Fig. 4.

A photograph of an experimental surface acoustic wave motor is shown in Fig. 5. The motor consists of fixed parts and a movable part. The stator and a linear guide rail were the fixed parts. The stator was held between a steel jig and a glass substrate; the steel jig had a glued rubber plate that contacts the stator. The linear guide rail was fixed to a steel block that was placed parallel to the stator.

The movable part was comprised of the silicon slider, a steel hemisphere, and a linear guide stage. The movable part moved along the linear guide rail. The steel hemisphere was made of a steel ball, a portion of which was

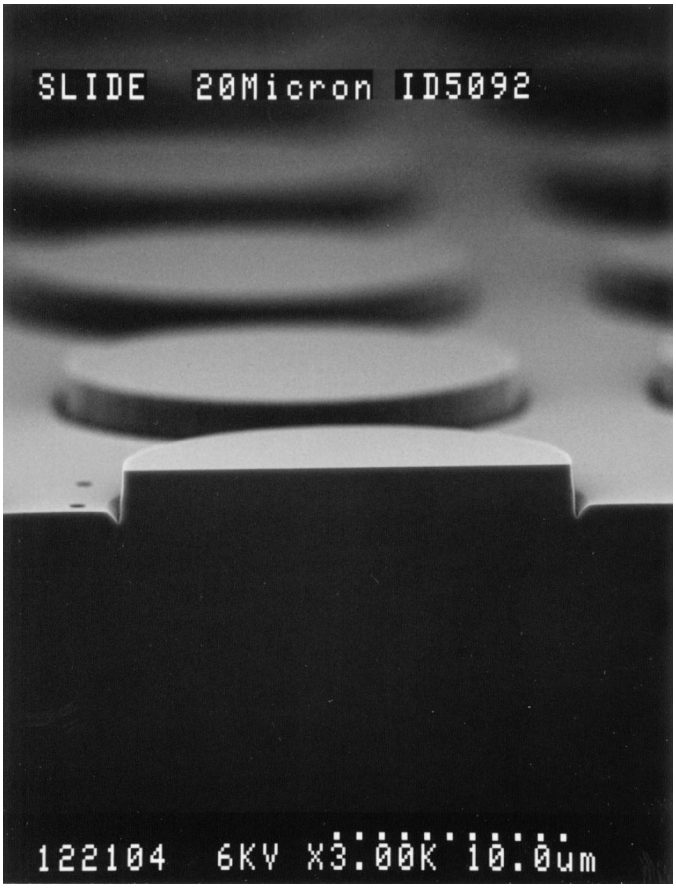

Fig. 4. Contact surface of the silicon slider having cylindrical projections of 20 μm in diameter and 2 μm in height.

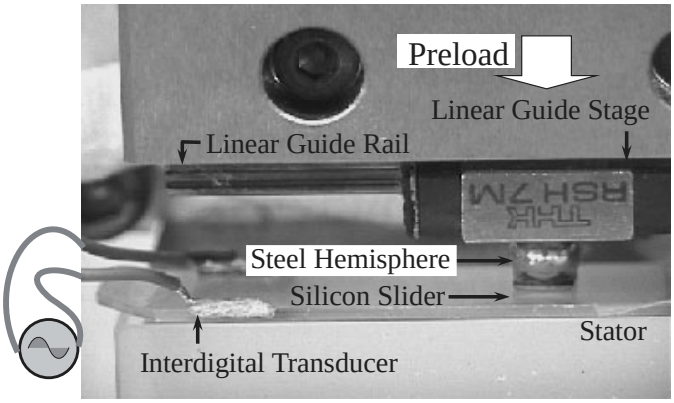

Fig. 5. The experimental surface acoustic wave motor.

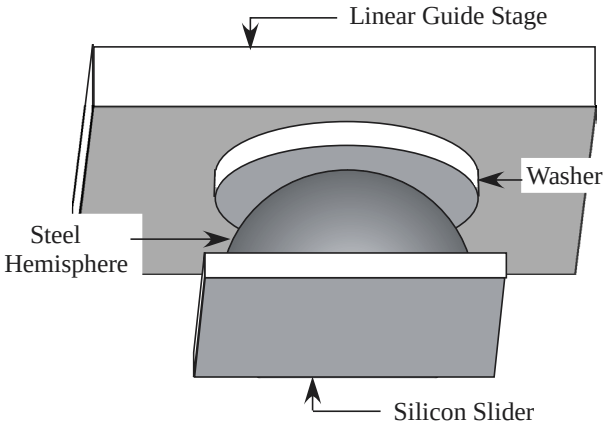

Fig. 6. Schema of the experimental setup's movable part.

scraped away in order to make a 4-mm diameter flat plane to enable the attachment of the silicon slider. Its shape was not a precise hemisphere, but it is simply called a hemisphere in this paper. The silicon slider was glued with epoxy resin onto the steel hemisphere. The steel hemisphere was put into a brass washer, which was glued with epoxy resin onto the linear guide stage. A hemisphere and washer connection mechanism were used to maintain the parallel contact between the silicon slider surface and the stator surface. The movable part is illustrated in Fig. 6.

A He-Ne laser beam of a laser Doppler interferometer was incident on the steel hemisphere in order to measure the stepping motions of the silicon slider. A signal processor of the interferometer (PI Polytec GmbH, Waldbronn, Germany VDD-650) demodulated the displacement of the slider up to a 2-picometer resolution. The frequency bandwidth of the demodulator was 0.3 Hz to 2 MHz.

The preload of the silicon slider was provided by a coil spring via the steel block with rotation of a micrometer head so that the preload could be adjusted easily. A photograph of the whole experimental setup, Fig. 7, shows the preload structure. The steel block, to which the linear guide rail was attached, was used to stabilize the preload independent of the position of the slider. The indicated rectangle in the photograph is the part of the surface acoustic wave motor indicated in Fig. 5. The preload was adjusted from 20 N to 40 N during the experiment.

IV. Stepping Motion

A. Driving Method and Slider Motion

Burst driving voltages were applied to the IDT every 0.2 ms to drive the surface acoustic wave motor in a stepping motion. The Rayleigh waves were generated by the IDT when the driving voltages were applied. The Rayleigh waves, therefore, were propagated intermittently every 0.2 ms. The movable part underwent repeated accelerations and decelerations, depending on whether or not the Rayleigh wave was propagating underneath the silicon slider.

A burst period of 0.2 ms was the minimum duration required for the slider to stop after a step motion. A waveform of the applied burst driving voltage is shown in Fig. 8. The driving voltage was adjusted from 90 V_{peak} to 120 V_{peak}, and the driving waves were varied from 20 cycles to 100 cycles. Thus, the duration while the driving voltage was applied was 10.4 μs at most.

An example of a stepping drive motion is shown in Fig. 9, in which the driving voltage was 100 V_{peak}, the driving waves were 50 cycles, and the preload was 30 N. Step motions were observed every 0.2 ms when the driving

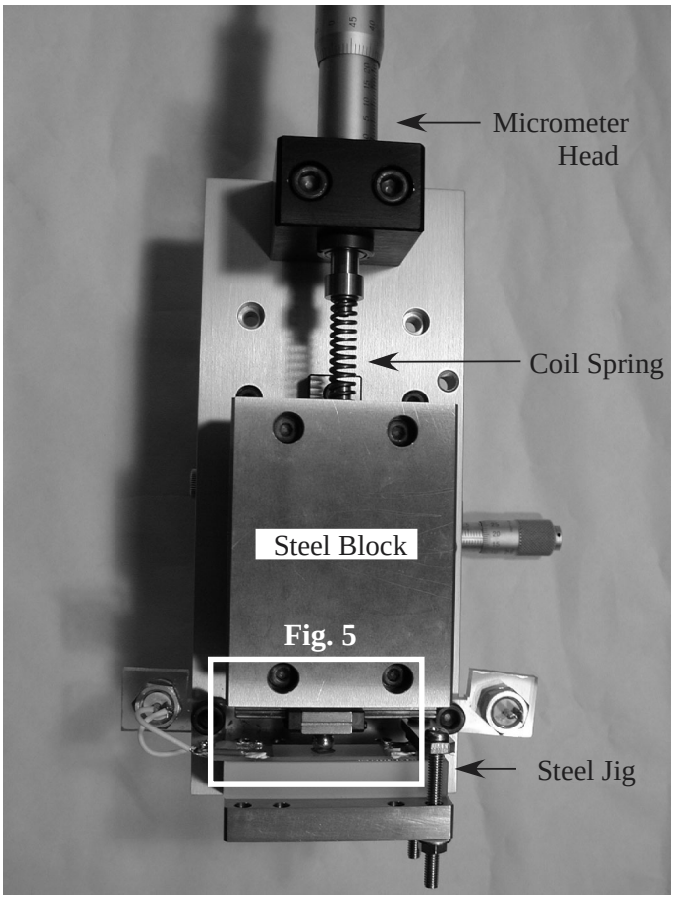

Fig. 7. The whole experimental setup.

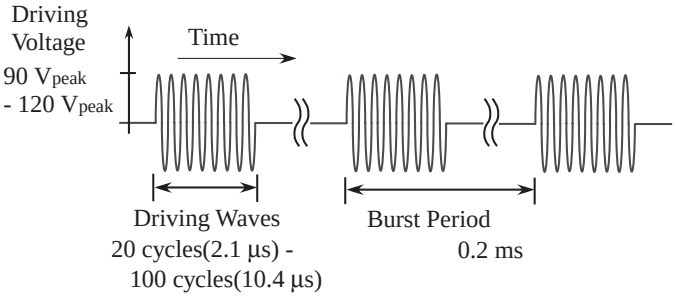

Fig. 8. A waveform of the burst driving voltage applied to the IDT.

voltages were applied. Each step displacement was about 20 nm. The mean traveling speed was about 100 μm/s in this 2 ms period. The distribution of the 10 steps shown in Fig. 9 was within 5%, and the variance was 0.41 nm^2.

B. Friction Drive and Step Size

Details of the stepping drive motion are shown in Fig. 10. This motion is an enlarged image of the motion shown in Fig. 9 in order to examine the process of the stepping motion more closely. When the driving voltage was applied, since the Rayleigh wave was excited, friction with the surface particles of the stator yielded the driving force to the silicon slider. The silicon slider accelerated rapidly

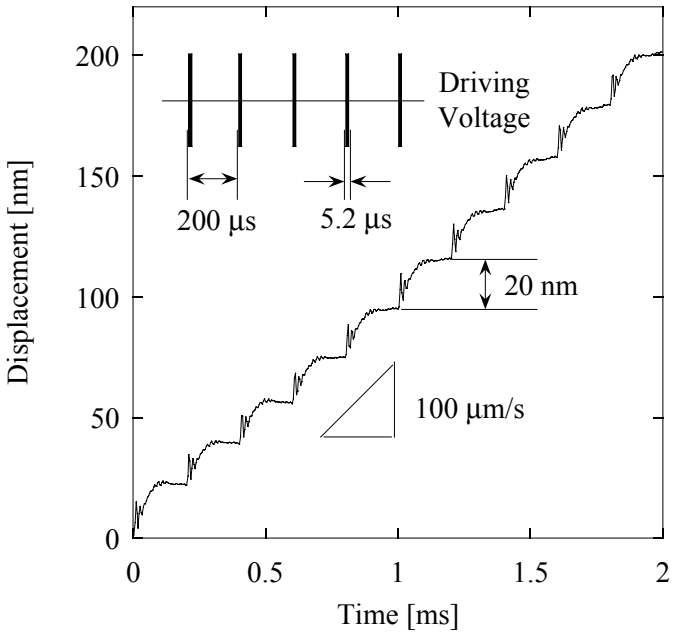

Fig. 9. An approximately 20-nm stepping drive motion; the driving voltage was 100 V_{peak}, the driving waves were 50 cycles, and the preload was 30 N. The burst period was 0.2 ms.

with the displacement then reaching its first peak. This moment occurred at almost the same time as the standstill of the Rayleigh wave. During the propagation of the Rayleigh wave, the silicon slider moved about 13 nm due to the friction driving force. This movement of the slider is defined as friction driven displacement in this paper. The friction driven displacement is indicated in Fig. 10 as the displacement that occurs when the driving voltage is applied. It is the actual driven displacement due to the friction driving force between the Rayleigh wave and the silicon slider.

Due to the inertia of the linear guide stage and the friction of the linear guide rail, the entire movable part moved more slowly than did the silicon slider part, that is, the slider and the glued steel hemisphere. As can be seen from the shoulder part of the enhanced step motion curve in Fig. 10, the silicon slider part dragged by the linear guide stage was forwarded accompanied by vibrations.

When the vibration of the silicon slider part diminished, the displacement of the silicon slider part was larger than that of the friction driven displacement. The displacement between the static point of the silicon slider and the starting point of the friction driven displacement provides for the step displacement as indicated in Fig. 10. The elastic connection between the steel hemisphere and the brass washer caused the difference between the friction driven displacement and the step displacement.

The experimental results indicated that the movable part of the experimental setup did not move as a single mass. Namely, the movable part behaved as two elastically connected masses; one was the silicon slider part that consisted of the silicon slider and the steel hemisphere that

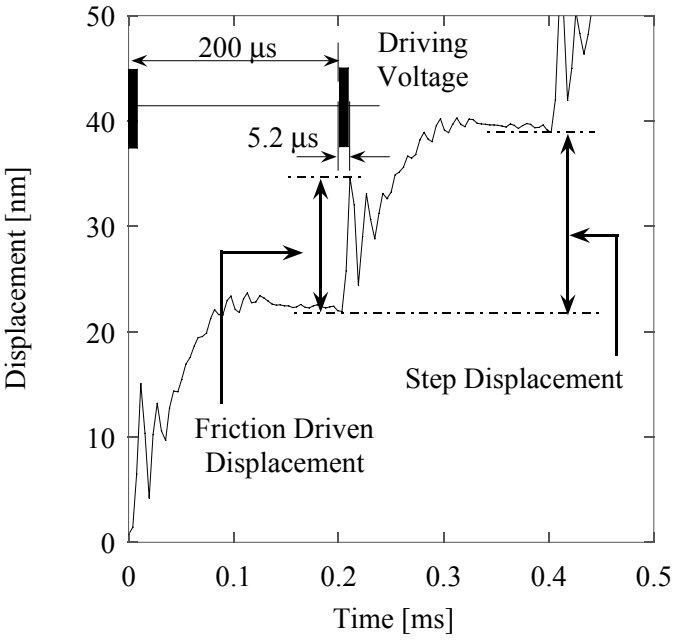

Fig. 10. Enhanced trace of the stepping drive motion shown in Fig. 9; the driving voltage was 100 V_{peak}, the driving waves were 50 cycles, and the preload was 30 N. The burst period was 0.2 ms.

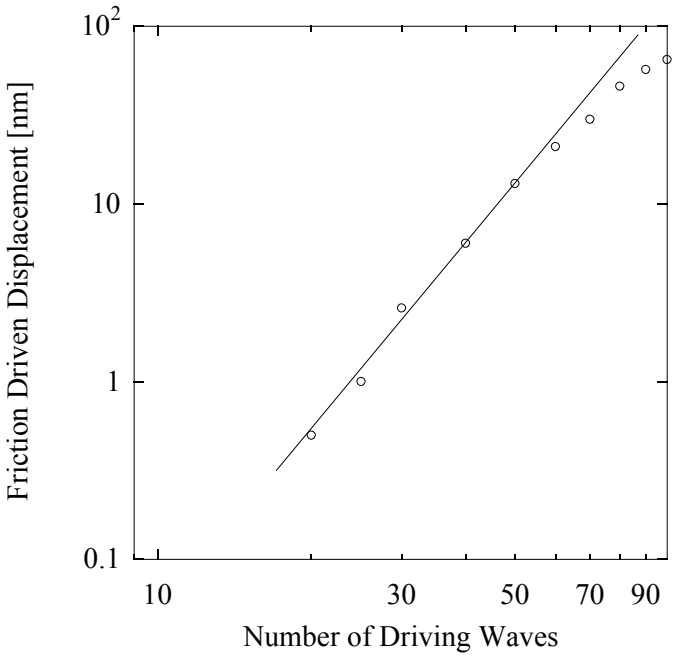

Fig. 11. Friction driven displacement in relation to the number of the driving waves; the driving voltage was 100 V_{peak} and the preload was 30 N.

weighed only 0.89 g, and the other was the linear guide stage that weighed 9.42 g.

A step displacement was the displacement affected by the inertia and the vibration after a friction drive. The kinetic energy generated by the friction drive was consumed by friction with the quiet stator and damper components of the elastic connection during the vibration. But the kinetic energy consumption during friction driven displacement happened to move the silicon slider part and to create an elastic deformation at the connection. The friction driven displacement indirectly indicated the power produced by the friction drive. Hence, instead of the step displacements, the friction driven displacements of stepping motions were measured in order to estimate the friction drive. The friction driven displacements in the following figures were the averages of eight steps after the unstable initial two steps, in a manner similar to the steps indicated in Fig. 9.

C. Friction Driven Displacement

The driving waves were varied from 20 cycles to 100 cycles; the driving voltage and the preload were maintained at 100 V_{peak} and 30 N, respectively. The friction driven displacement in relation to the number of driving waves is shown in Fig. 11. The friction driven displacement increased with the square of the number of the driving waves up to 60 cycles of the driving waves, or 20 nm of the displacement. The rate of increase of the friction driven displacement then lessened. The stored kinetic energy at the elastic connection increased with the square of the elastic deformation at that point in the manner of a coil spring. Namely, the effect of the elastic deformation emerged over a range of several tens of nanometers. A friction driven displacement of 0.5 nm was obtained at 20 cycles of the driving waves.

The driving voltage was varied from 90 V_{peak} to 120 V_{peak}, and the driving waves were adjusted from 40 cycles to 80 cycles; the preload was 30 N. The friction driven displacement in relation to the driving voltage is shown in Fig. 12. The friction driven displacement increased with the square of the driving voltage under each driving wave condition.

The preload was varied from 20 N to 40 N; the driving voltage was 100 V_{peak} and the driving waves were set from 40 cycles to 80 cycles. The friction driven displacement in relation to the preload is shown in Fig. 13. The friction driven displacement decreased with the increase of the preload.

V. Nanometer Stepping Drives

Changing the number of the driving waves is the easiest way to determine the desired stepping motion under the open loop condition. The friction driven displacement increased with the square of the number of the driving waves as previously shown in Fig. 11. Accordingly, the highest resolution stepping drives were examined by means of the reduction of the driving waves; the driving voltage and the preload were maintained at 100 V_{peak} and 30 N. By applying the 40 cycles of the driving waves, an approximately 8-nm stepping drive motion was obtained as illustrated in Fig. 14. This was the highest resolution stepping motion we obtained without signal processing the measured data. Owing to the drift of the laser Doppler interferometer, the measured motion data included fluctuations of about 5 to

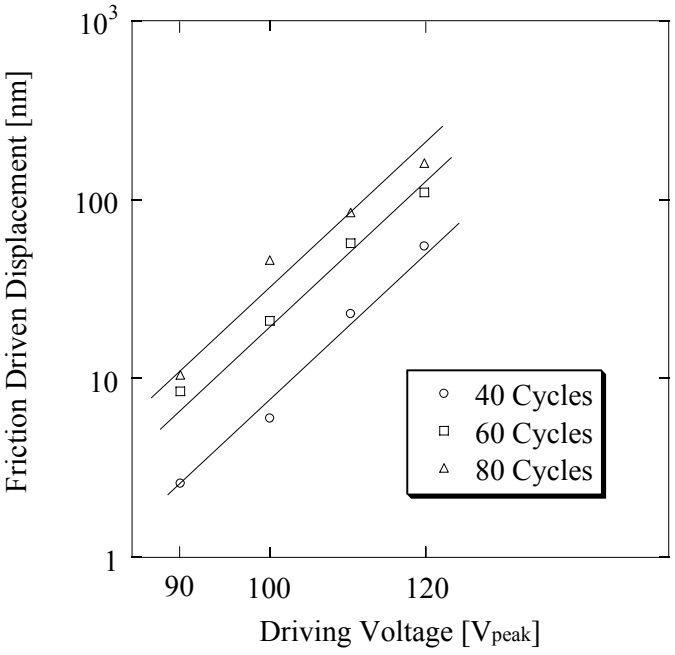

Fig. 12. Friction driven displacement in relation to the driving voltage; the driving wages were 40, 60, and 80 cycles, and the preload was 30 N.

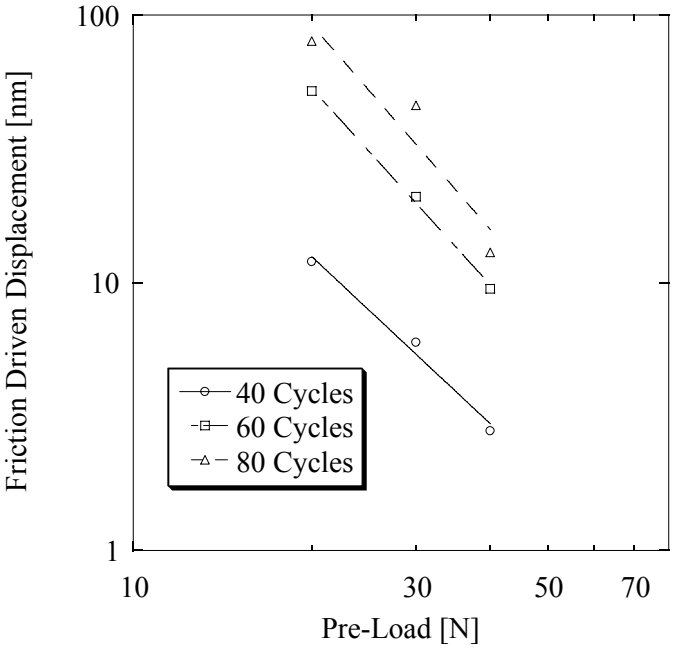

Fig. 13. Friction driven displacement in relation to the preload; the driving voltage was 100 V_{peak}, and the driving waves were 40, 60, and 80 cycles.

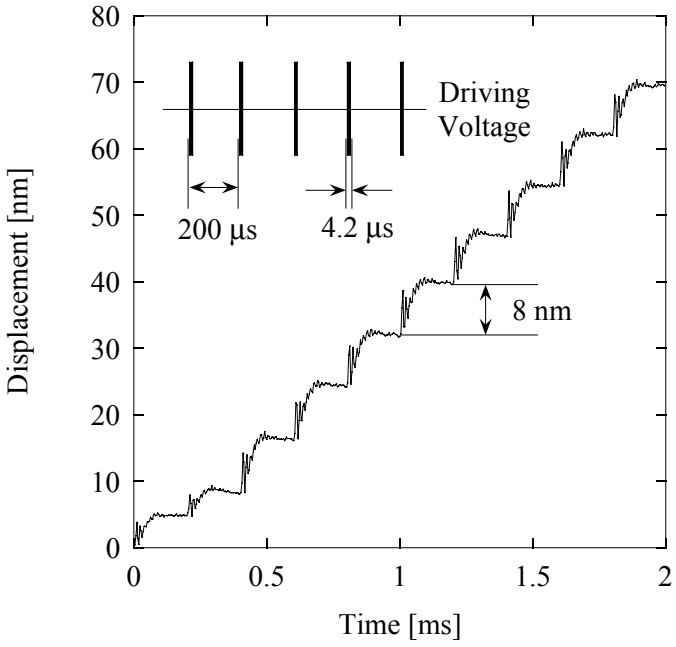

Fig. 14. The 8-nm stepping drive motion; the driving voltage was 100 V_{peak}, the driving waves were 40 cycles, and the preload was 30 N. The burst period was 0.2 ms.

10 nm independent to the slider motion. Therefore, it was uncertain whether data of a stepping drive motion less than 5 nm could be obtained using a single-shot measurement.

For observation of the higher resolution stepping motion of the silicon slider, measured motion data were averaged. Fig. 15 shows the stepping drive motion when applying 25 driving waves, as the driving voltage was 100 V_{peak} and the preload was 30 N. The data indicates the average of 28 stepping drive motions. The step displacement was approximately 2 nm, and the friction driven displacement was approximately 1 nm. This stepping motion was the highest resolution stepping motion of the experimental setup. The inertia and the vibration due to the elastic deformation were significant in these nanometer ranges of stepping drive motions. The beginning several cycles of the vibration following the friction drive had almost the same amplitude as did the friction driven displacement.

As shown in Fig. 16, vibration became a problem at the subnanometer stepping drive range. Fig. 16 shows the stepping drive motion with the application of 20 driving waves; the driving voltage was 100 V_{peak} and the preload was 30 N. The indicated data was also the average motion of 30 stepping drive motions. A mean traveling motion of 0.5 nm in each step accompanied by subnanometer vibration was observed. The friction driven displacement and the vibration amplitude caused by the elastic deformations were of similar quantity throughout the stepping motion. This motion no longer can be considered stepping motion, but a 0.5 nm friction driven displacement was observed when the driving voltage was applied. Namely, the subnanometer stepping motion was masked by vibration due to the compliance of the structure.

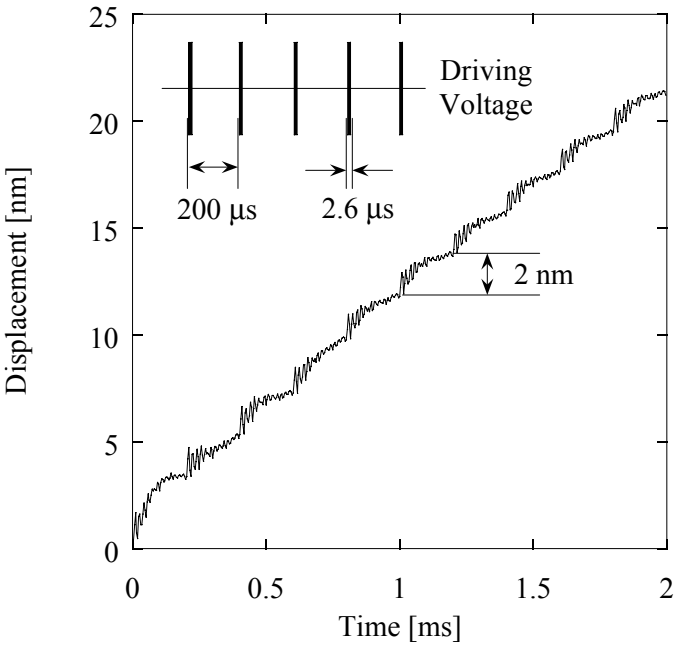

Fig. 15. The highest resolution stepping drive motion, 2-nm stepping motion, of the experimental setup; the driving voltage was 100 V_{peak}, the driving waves were 25 cycles, and the preload was 30 N. The burst period was 0.2 ms. The traced data was the average of 28 motions.

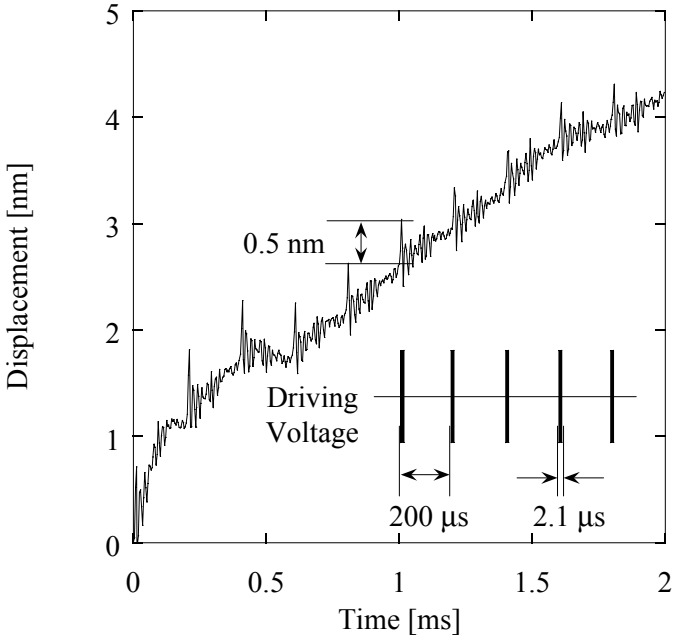

Fig. 16. Subnanometer stepping drive motion; the friction driven displacement was about 0.5 nm. The driving voltage was 100 V_{peak}, the driving waves were 20 cycles, and the preload was 30 N. The burst period was 0.2 ms. The traced data was the average of 30 motions.

VI. Confirmation

Brass is a soft metal whose Young's modules is about 100 [GPa]. To reduce the vibrations caused by the elastic deformation at the connection, the brass washer was replaced with a stainless steel (SUS304, JIS Japanese Standards Association, Tokyo, Japan) washer whose Young's modules is 197 [GPa]. The linear guide also was replaced with a less friction-inducing linear guide.

For the investigation of the motor stepping drive's dependency on time or total displacement, the measurement time range was changed from 4 ms to 400 ms. The conditions of the stepping drives were 100 V_{peak} driving voltage, 40 cycles of driving waves, and 30 N of preload. The measured data are drawn in Fig. 17. Each graph shows a mean traveling speed of approximately 250 μm/s. In Fig. 17(c), an approximately 50-nm stepping motion was verified. Consequently, the stepping motions were constant up to the range of several hundreds of milliseconds or several hundreds of micrometers.

The stepping motion of the linear guide stage also was measured at the stepping drive, in which the driving voltage, the driving waves, and the preload were 100 V_{peak}, 40 cycles, and 30 N, respectively. The linear guide stage responded slowly with delay, as shown in Fig. 18. The peaks of the steps of the linear guide stage were larger than the step displacements of the silicon slider. The friction driven displacement caused an elastic deformation at the elastic connection between the washer and the hemisphere, and the restoring force of the elastic deformation then drove both the silicon slider part and the linear guide stage. Because the mass of the linear guide stage was about 10 times larger than that of the silicon slider part, the motion of the linear guide stage was larger in amplitude at a lower frequency than was that of the silicon slider.

Nanometer-order stepping motion was examined with this structure in order to specify the effect of the stiff washer. Fig. 19 shows the stepping motion of the silicon slider under a 100 V_{peak} driving voltage, 13 cycles of driving waves, and a 30 N preload condition. The data indicates the average of 30 stepping drive motions. Approximately 2-nm step motions were obtained. The friction driven displacement was relatively smaller, about 0.5 nm, than the 2-nm stepping drive with the brass washer structure as indicated in Fig. 15, in which the friction driven displacement was about 1 nm. The vibration amplitude after the friction driven displacement diminished with the use of the stiff washer. However, the inertia of the heavy linear guide stage was more significant in this stepping motion as seen in that the light silicon slider part was pulled back after the peak of the step displacement.

VII. Discussion

Fig. 20 shows a simplified mechanical model of the movable part, taking into account the compliance of the structure. A spring and a damper produce an elastic connec-

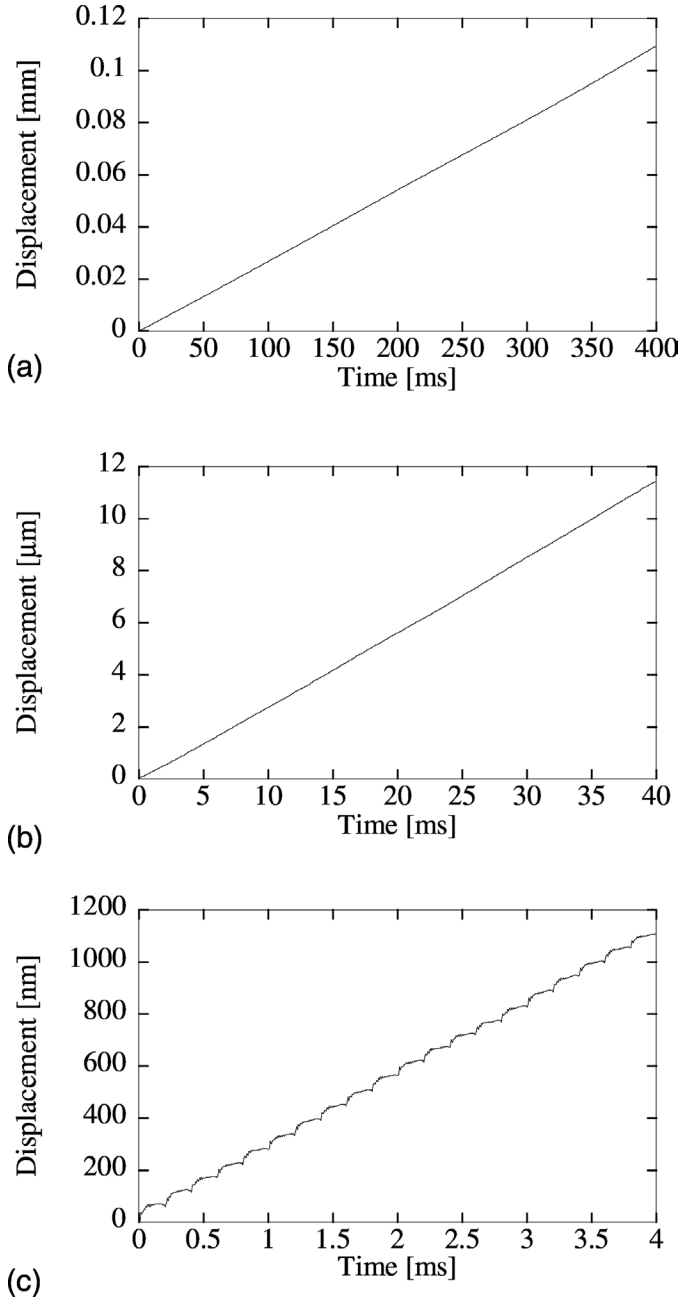

Fig. 17. Stepping drive motions; the driving voltage was 100 V_{peak}, the driving waves were 40 cycles, and the preload was 30 N. The burst period was 0.2 ms. The time range of the measured motions were (a) 400 ms, (b) 40 ms, (c) 4 ms.

tion between the steel hemisphere and the washer. When the Rayleigh wave is excited, the driving force on the silicon slider compresses the spring, which in turn pushes the linear guide stage. After the Rayleigh wave passes away, there is no driving force acting on the silicon slider, and the silicon slider then is thrust back by the elastic force of the compressed spring. In this way, the silicon slider part, namely the silicon slider and the glued hemisphere, begins to vibrate at a certain frequency according to the mass of the silicon slider part and the elastic constant of the spring.

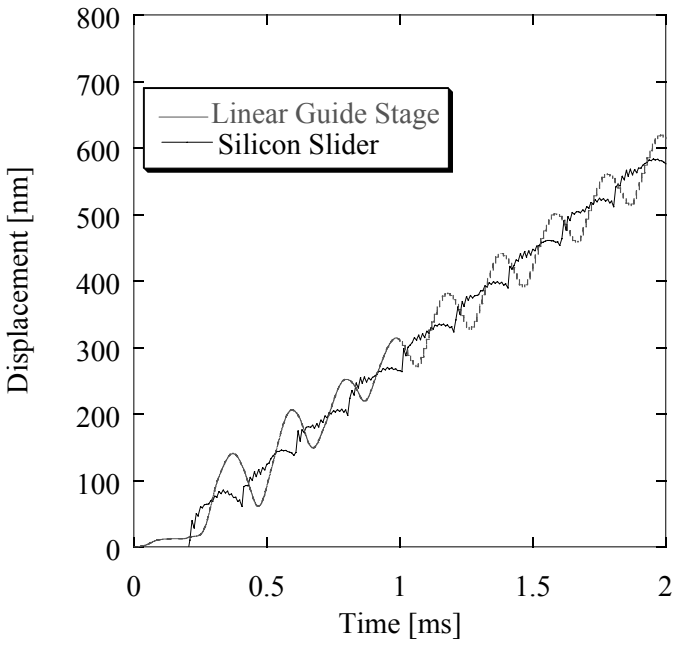

Fig. 18. Stepping drive motion of the linear guide stage and the silicon slider; the driving voltage was 100 V_{peak}, the driving waves were 40 cycles, and the preload was 30 N. The burst period was 0.2 ms.

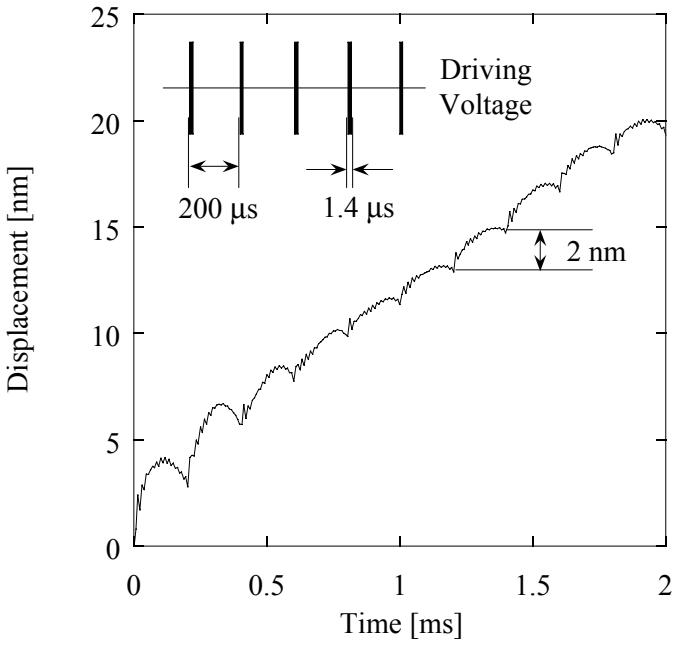

Fig. 19. The 2-nm stepping drive motion using the stainless washer structure; the driving voltage was 100 V_{peak}, the driving waves were 13 cycles, and the preload was 30 N. The burst period was 0.2 ms. The indicated data was the average of 30 motions.

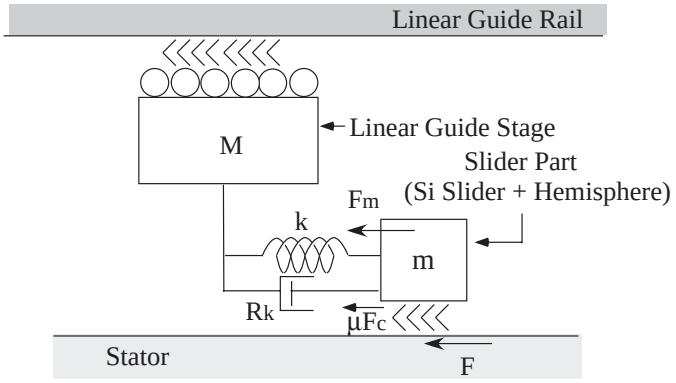

Fig. 20. A simplified mechanical model of the movable part.

However, the linear guide stage is pushed by the compressed spring, which is driven by the first movement of the silicon slider part. As previously indicated, the masses of the linear guide stage and the silicon slider part were 9.42 and 0.89 g, respectively. The mass of the linear guide stage was about 10 times larger than that of the silicon slider part. According to the larger mass, hence, the vibration of the linear guide stage occurs at a lower frequency.

The damper component of the elastic connection between the hemisphere and the washer suppresses the vibrations of the silicon slider part and the linear guide stage. The frictional force between the silicon slider and the nonwavy stator diminishes the higher frequency nanometer-order vibrations of the silicon slider part. The frictional force between the linear guide stage and the linear guide rail diminishes the lower frequency vibrations of the linear guide stage.

The equivalent model in Fig. 20 includes major physical factors. The numerical values of each element should be evaluated based on experimental results regarding vibration frequencies and decays. Numerical simulations will deepen our understanding of these phenomena and will provide data essential for designing a subnanometer-resolution linear stage.

VIII. Conclusions

Nanometer stepping drives of a surface acoustic wave motor were examined. The highest resolution stepping drive motion of the experimental setup was a 2-nm stepping motion. Although the subnanometer stepping motion was masked by vibration, the possibility of subnanometer resolution was indicated. The need for vibration reduction due to the structural compliance then was pointed out. Thus, a structure in which a movable part moves as a single mass needs to be designed. This rigid structure will be able to perform a high-resolution, subnanometer stepping motion.

References

[1] V. Snikta, "Ultrasonic actuators for nanometer positioning," *Ultrason.*, vol. 38, pp. 20–25, 2000.

[2] M. Umeda, T. Nakazawa, K. Ohnishi, K. Nakamura, M. Kurosawa, and S. Ueha, "Positioning characteristics of ultrasonic rotary actuator with two mode operation," in *Proc. IEEE Ultrason. Symp.*, pp. 1201–1204, 1990.

[3] http://www.nanomotion.net, Yokneam, Israel: Nanomotion Ltd.

[4] C.-H. Yun, T. Ishii, K. Nakamura, S. Ueha, and K. Akashi, "A high power ultrasonic linear motor with a longitudinal-bending hybrid transducer for high-speed and precise drive of a heavy stage," in *Proc. IEEE Ultrason. Symp.*, pp. 537–540, 2001.

[5] M. K. Kurosawa, O. Kodaira, Y. Tsuchitoi, and T. Higuchi, "Transducer for high speed and large thrust ultrasonic linear motor using two sandwich type vibrator," *IEEE Trans. Ultrason., Ferroelect., Freq. Contr.*, vol. 45, no. 5, pp. 1188–1195, 1998.

[6] M. Kurosawa, M. Takahashi, and T. Higuchi, "Ultrasonic linear motor using surface acoustic waves," *IEEE Trans. Ultrason., Ferroelect., Freq. Contr.*, vol. 43, no. 5, pp. 901–906, 1996.

[7] N. Osakabe, M. Chiba, M. Kurosawa, and T. Higuchi, "Experimental estimation of surface acoustic wave linear motor," in *Proc. Int. Conf. Micromech. Information Precision Equipment*, pp. 265–268, 1997.

[8] M. K. Kurosawa, M. Chiba, and T. Higuchi, "Evaluation of a surface acoustic wave motor with a multi-contact-point slider," *Smart Mater. Struct.*, vol. 7, pp. 305–311, 1998.

[9] K. Asai, M. K. Kurosawa, and T. Higuchi, "Evaluation of the driving performance of a surface acoustic wave linear motor," in *Proc. IEEE Ultrason. Symp.*, pp. 675–679, 2000.

[10] M. K. Kurosawa and T. Higuchi, "Surface acoustic wave motor," in *Proc. 3rd Int. Heintz Nixdorf Symp.*, pp. 113–118, 1999.

[11] M. K. Kurosawa, "State-of-the-art surface acoustic wave motor and its future applications," *Ultrason.*, vol. 38, pp. 15–19, 2000.

[12] M. K. Kurosawa, H. Itoh, K. Asai, M. Takasaki, and T. Higuchi, "Optimization of slider contact face geometry for surface acoustic wave motor," in *Proc. IEEE Int. Symp. Micro Electro Mech. Syst.*, pp. 252–255, 2001.

[13] M. K. Kurosawa, M. Takahashi, and T. Higuchi, "Elastic contact conditions to optimize friction drive of surface acoustic wave motor," *IEEE Trans. Ultrason., Ferroelect., Freq. Contr.*, vol. 45, no. 5, pp. 1229–1237, 1998.

[14] T. Maeno and D. B. Bogy, "Effect of the hydrodynamic bearing on rotor/stator contact in a ring-type ultrasonic motor," *IEEE Trans. Ultrason., Ferroelect., Freq. Contr.*, vol. 39, no. 6, pp. 675–682, 1992.

[15] N. Osakabe, M. Kurosawa, T. Higuchi, and O. Shinoura, "Surface acoustic wave linear motor using silicon slider," in *Proc. IEEE Workshop Micro Electro Mech. Syst.*, pp. 390–395, 1998.

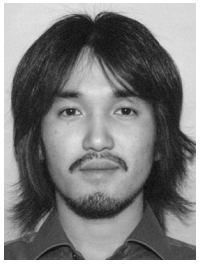

Takashi Shigematsu was born in 1977. He received the B.Eng. degree in electrical and electronic engineering from Tokyo Institute of Technology, Tokyo, Japan in 2001. He is currently a master course student of the Interdisciplinary Graduate School of Engineering, Tokyo Institute of Technology. He is a student member of the Institute of Electronics Information and Communication Engineers, and IEEE.

Minoru Kuribayashi Kurosawa (formerly Kuribayashi) (M'95) was born in Nagano, Japan, on April 24, 1959. He received the B.Eng. degree in electrical and electronic engineering, and the M.Eng. and D.Eng. degrees from Tokyo Institute of Technology, Tokyo, in 1982, 1984, and 1990, respectively.

Beginning in 1984, he was a research associate of the Precision and Intelligence Laboratory, Tokyo Institute of Technology, Yokohama, Japan. From 1992, he was an associate professor at the Department of Precision Machinery Engineering, Graduate School of Engineering, The University of Tokyo, Tokyo, Japan. Since 1999, he has been an associate

professor at the Department of Advanced Applied Electronics, Interdisciplinary Graduate School of Engineering, Tokyo Institute of Technology, Yokohama, Japan. His current research interests include ultrasonic motor, micro actuator, PZT thin film, SAW actuator, and single bit digital signal processing and its application to control system.

Dr. Kurosawa is a member of the Institute of Electronics Information and Communication Engineers, the Acoustical Society of Japan, IEEE, the Institute of Electrical Engineers of Japan, and the Japan Society for Precision Engineering.

Katsuhiko Asai was born in 1970. He received the B.S. and M.S. degrees in mechanical engineering from Tokyo Institute of Technology, Tokyo, Japan in 1992 and 1994, respectively. He joined Matsushita Electric Industrial Co., Ltd., Osaka, Japan in 1994. He has been engaged in research and development of SAW actuator.